Supplementary Material

Anomalous diffusion for active Brownian particles cross-linked to a networked polymer: Langevin dynamics simulation and theory

Sungmin Joo,[1] Xavier Durang,[1] O-chul Lee,[1] and Jae-Hyung Jeon[1]

[1]*Department of Physics, POSTECH, Pohang 37673, Republic of Korea*

Abstract

This Supplementary Material contains additional figures and analytic results which further illustrate the point made in the main text.

I. SUPPLEMENTARY FIGURES

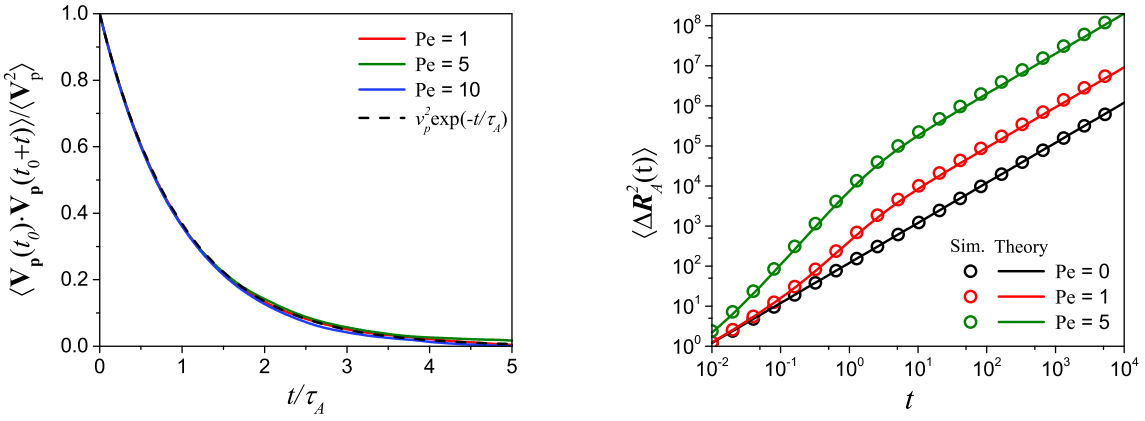

FIG. S1: Preliminary simulations testing the dynamics of an active Brownian particle (ABP) in free space. (Left) The autocorrelation property of the propulsion velocity $\mathbf{V}_{\rm p}(t)$ of an ABP simulated at Pe $=$ 1, 5, and 10 is shown. In our model, the self-propulsion of the ABP is modeled by an active noise of the Ornstein-Ulhlenbeck (OU) type and generated in the simulation using Eq. (4) in the main text. The simulation data are then compared to the theoretical expectation (dashed line) $\langle \mathbf{V}_{\rm p}(t_0)\cdot\mathbf{V}_{\rm p}(t_0+t)\rangle = v_{\rm p}^2\exp(-t/\tau_A)$ with the input correlation time $\tau_A = 1$. (Right) The MSD of a single ABP in free space at Pe $= 0$, 1, and 5. We validate our simulation code via the simulation of an ABP in free space using Eq. (1) and compare the MSDs with the theoretical curve. The simulation data (symbol) are in excellent agreement with the analytical theory $\langle \Delta\mathbf{R}^2(t)\rangle = 6Dt + 2v_{\rm p}^2\tau_A^2\left(t/\tau_A + e^{-t/\tau_A} - 1\right)$. The ABP has a self-propelled dynamics $\sim t^2$ for $t \ll \tau_A$ and beyond this time scale shows an athermal Fickian motion with a diffusivity $D_{\rm eff} = D + v_{\rm p}^2\tau_A/3$.

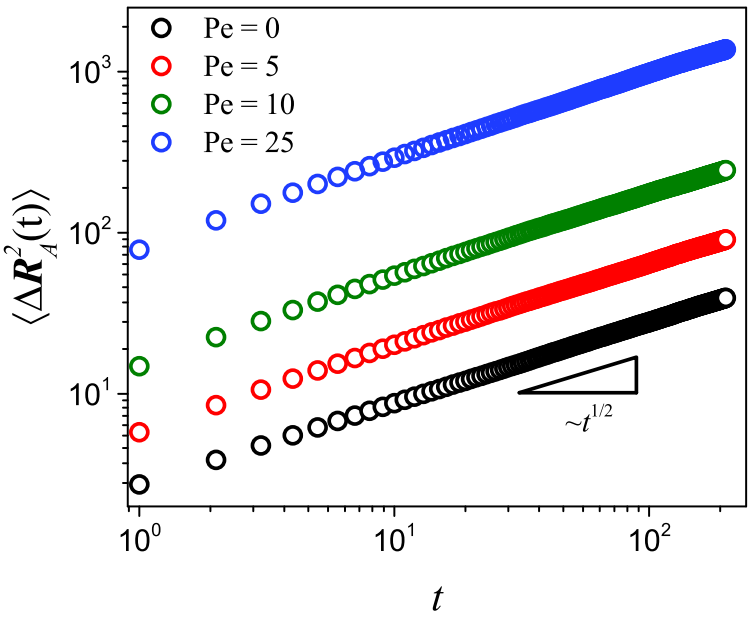

FIG. S2: Dynamics of the active star polymers where all beads are of the same ABP. These systems are simulated for the star polymers with the functionality $f = 3$, the length of the arm chain $N = 100$, and Pe $= 0,\ 5,\ 10$, and 25. In the plot, the MSDs of the cross-linkers for the four Pe conditions are presented. The results show that, contrary to the systems studied in the main text, the cross-linkers in this system always exhibit the Rouse-like subdiffusion $\sim t^{1/2}$ for any Péclet numbers. Regarding this behavior, we provide the analytic theory in Sec. II B in the Supplementary Material.

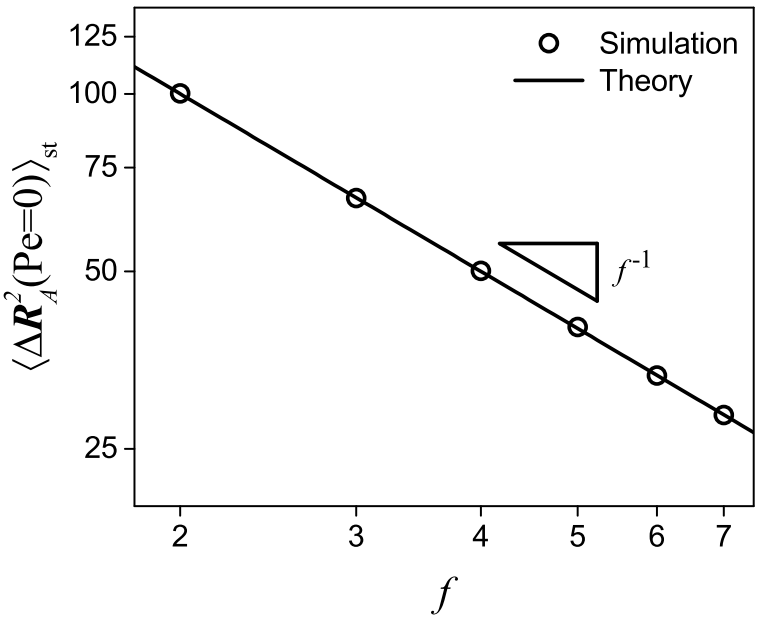

FIG. S3: The MSD of the Brownian cross-linker at the stationary state vs. f. The data (symbol) is for the star polymer with the fixed boundary conditions and $N = 100$. The solid line represents the expected theory $\langle \Delta \mathbf{R}_A^2(\mathrm{Pe} = 0) \rangle_{\mathrm{st}} = 6Nk_BT/fk$ [1], illustrating the scaling relation for MSD decaying as $1/f$ with the functionality.

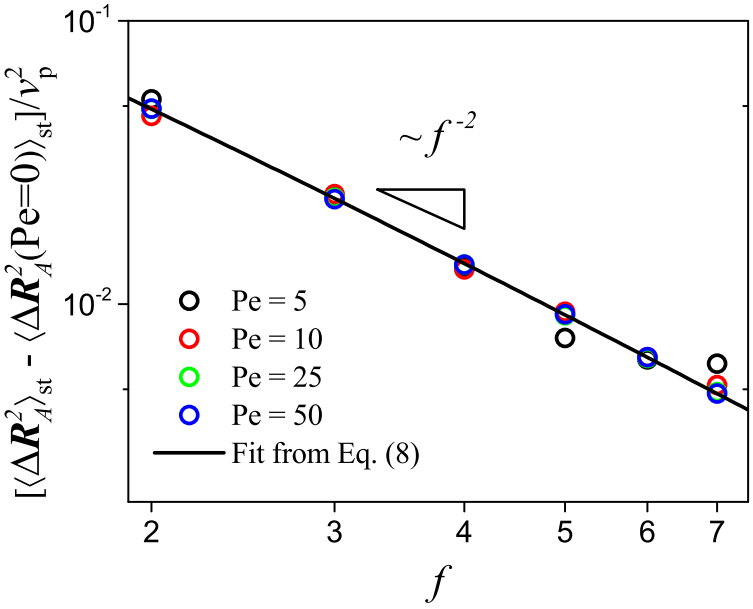

FIG. S4: The stationary value of MSD vs. f. Here the plotted MSD is contributed to solely by the active noise, divided by v_p^2. All the data at different Pe values collapse onto each other. The solid line shows the fit to the data with the corresponding theoretical expression in Eq. (8) [main text]. The data scales approximately as f^{-2}.

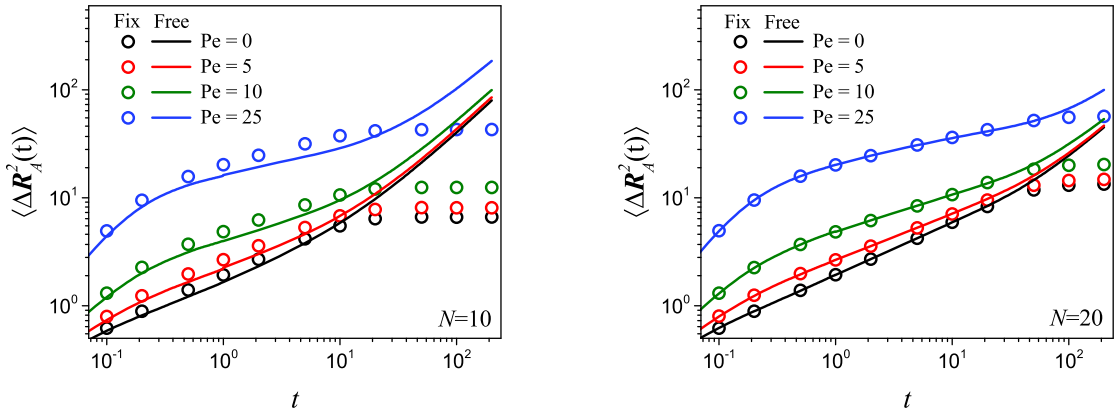

FIG. S5: The MSDs for the ABP cross-linker for $N = 10$ (Left) and $N = 20$ (Right). As shown in the main text (Fig. 7), the dynamics of ABP cross-linker at $t \lesssim \tau_R$ does not depend on the conditions of the boundary as long as the length of the arm N is sufficiently long (e.g., $N = 100$ in the ABP-polymer system considered in the main text). Here, the supplementary simulations show that the boundary-free ABP dynamics at $t \lesssim \tau_R$ is preserved until the arm length is decreased to $N = 20$ (Right). When N is decreased as short as $N = 10$ (Left), the dynamics of ABP cross-linker depends on the boundary conditions. The simulation parameters are the same as in Fig. 7.

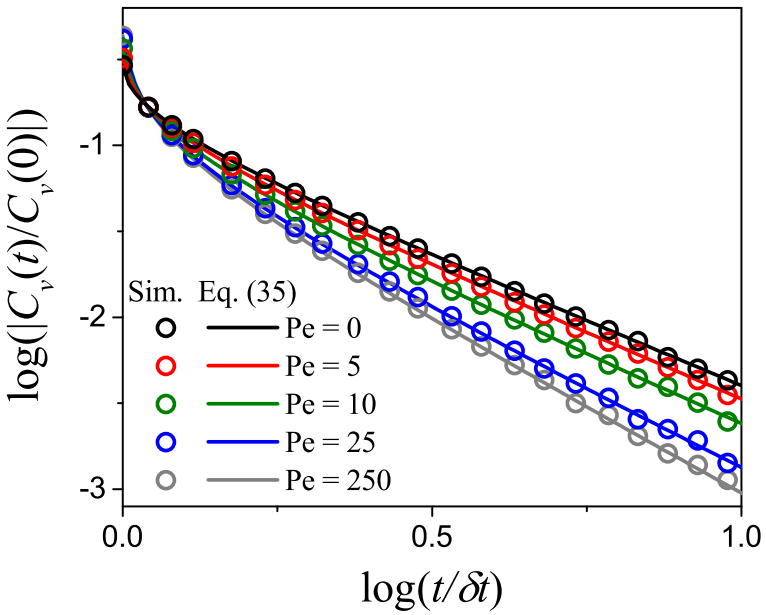

FIG. S6: Comparison between the theoretical VACF curves (solid line) and the VACFs obtained from the simulation (symbol) for the ABP cross-linker for $t \geq \delta t$. The theoretical lines are obtained by numerically evaluating Eq. (35) [main text]. In the simulation, we use $f = 2$ and $N = 100$. Our theory Eq. (35) excellently explains the VACFs in the simulation for various Pe conditions.

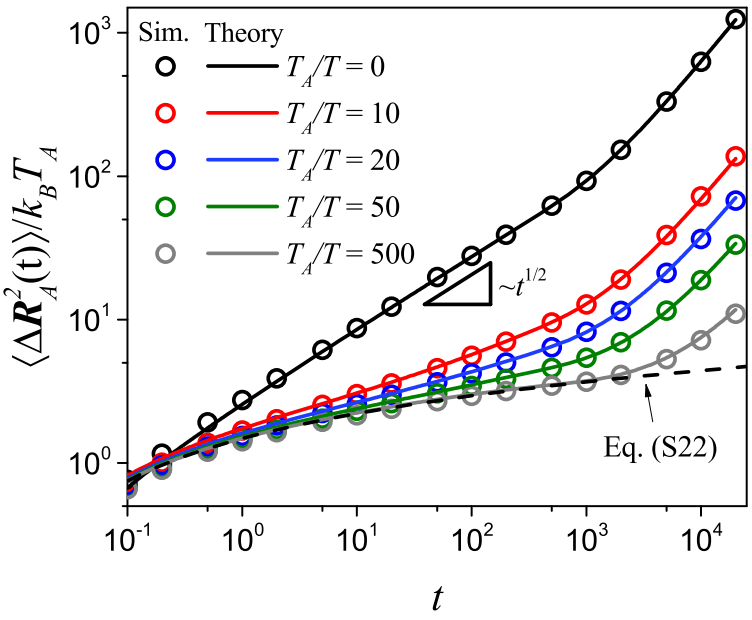

FIG. S7: Simulation results for a new ABP-polymer system where the active cross-linker is governed by an athermal white gaussian noise (WGN). In this plot, the MSDs for the ABP cross-linker in a polymer ($f = 2$) with the free boundary conditions are presented. Refer to Sec. II D in the Supplementary Material for further information about this system and the WGN introduced. The strength of the WGN is controlled by its effective temperature T_A; see the definition of T_A in Eq. (S18). In the simulation above, the active temperature is increased from $T_A/T = 0$ to $T_A/T = 500$. The solid line depicts the analytic expectation of the MSD obtained as the sum of Eqs. (S19), (S20), and (S22). Note that the ABP cross-linker of this model also has a logarithmic growth ($\sim \ln t$) in MSD at a higher T_A condition [e.g., the case for $T_A/T = 500$]. The expected limiting MSD curve is Eq. (S22), shown in the dashed line above.

II. SUPPLEMENTARY THEORETICAL ANALYSIS

A. Numerical implementation for Langevin dynamics simulation

In this section, we describe in detail the numerical implementation for the Langevin dynamics simulations performed in this work. The equation of motion and the simulation variables shown below are given in terms of the basic length $[\sigma] = b$ (the bead diameter), time $[\tau] = [b^2/D]$ (D: the diffusivity), and the energy $[\varepsilon] = k_B T$ ($T = 300$ K).

The original governing Langevin equation (5) in the main text can be rewritten as in the following discrete form for simulation:

$$\begin{aligned} \mathbf{V}(t) &= F(\{\mathbf{R}(t)\}) + \mathbf{V}_{\text{th}}(t) + \mathbf{V}_{\text{p}}(t), \\ \mathbf{R}(t+\Delta t) &= \mathbf{R}(t) + \mathbf{V}(t)\Delta t. \end{aligned} \tag{S1}$$

In this expression, for simplicity we drop down the bead index. $\mathbf{V}(t)$ and $\mathbf{R}(t)$, respectively, denote the velocity and the position of a given monomer at time t; $F(\{\mathbf{R}(t)\})$ is the velocity from the deterministic forces from the harmonic interactions, namely, $F = -k\sum_{l=1}^{f}\left(\mathbf{R}_0(t) - \mathbf{R}_1^{(l)}(t)\right)$ for the center ABP cross-linker and $F = -k\left(2\mathbf{R}_i^{(l)}(t) - \mathbf{R}_{i+1}^{(l)}(t) - \mathbf{R}_{i-1}^{(l)}(t)\right)$ for the i-th bead in the l-th arm chain. $\mathbf{V}_{\text{th}}(t)$ is the random velocity from the thermal noise, numerically obtained from a gaussian distribution with the variance $\sqrt{6k_BT/[\gamma\Delta t]}$. $\mathbf{V}_{\text{p}}(t) = \boldsymbol{\eta}(t)/\gamma$ is the propulsion velocity for the ABP cross-linker while $\mathbf{V}_{\text{p}} = 0$ for the Brownian beads in the polymer network. In the simulation the propulsion velocity is generated independently from the governing equation (4) introduced in the text, i.e.,

$$\frac{d\mathbf{V}_{\text{p}}(t)}{dt} \equiv \mathbf{V}'_{\text{p}}(t) = -\tau_A^{-1}\mathbf{V}_{\text{p}}(t) + \sqrt{\frac{2v_{\text{p}}^2}{\tau_A}}\boldsymbol{\zeta}(t), \tag{S2}$$

where τ_A is the correlation time of the active OU noise, $\boldsymbol{\zeta}(t)$ the white gaussian noise with a variance $\sqrt{1/\Delta t}$, and v_{p} is the amplitude of the propulsion velocity. From Eq. (S2) the propulsion velocity at the next time step is updated by the rule

$$\mathbf{V}_{\text{p}}(t+\Delta t) = \mathbf{V}_{\text{p}}(t) + \mathbf{V}'_{\text{p}}(t)\Delta t. \tag{S3}$$

The autocorrelation of the propulsion velocity then satisfies the relation $\langle \mathbf{V}_{\text{p}}(t_1)\cdot\mathbf{V}_{\text{p}}(t_2)\rangle = v_{\text{p}}^2\exp(-|t_1-t_2|/\tau_A)$, see Fig. S1.

For the numerical integration of the stochastic equation (5) in the main text, we use the second-order Runge-Kutta algorithm (particularly, the Heun's method [2]). In this algorithm, we first

calculate the intermediate position $\hat{\mathbf{R}}$ and velocity $\hat{\mathbf{V}}$ at $t+\Delta t$ from the position and velocity at t via the relation:

$$\begin{aligned}\hat{\mathbf{R}}(t+\Delta t) &= \mathbf{R}(t)+\mathbf{V}(t)\Delta t,\\ \hat{\mathbf{V}}(t+\Delta t) &= F(\{\hat{\mathbf{R}}(t+\Delta t)\})+\mathbf{V}_{\mathrm{th}}(t)+\mathbf{V}_{\mathrm{p}}(t).\end{aligned} \tag{S4}$$

Then, the position of the particle at $t+\Delta t$ is obtained to

$$\mathbf{R}(t+\Delta t) = \mathbf{R}(t)+\frac{1}{2}\left(\mathbf{V}(t)+\hat{\mathbf{V}}(t+\Delta t)\right)\Delta t. \tag{S5}$$

In order to remove the initial condition dependence, in the simulation the systems are relaxed during the period of $10^4\tau$, which is longer than the Rouse time scale τ_R of the system. All the statistics are obtained after the relaxation process.

For the simulations with the fixed boundary condition, we fixed the end points on a circle of radius $bN^{1/2}$, which is the average end-to-end distance of the arm chain. It turns out that the position of the ends is irrelevant for the simulation results.

B. Dynamics of active Rouse chain

We study the collective dynamics of an active polymer system where all the beads are the same active Brownian particles (ABPs) considered in the main text. Recall that we have simulated this system and measured the MSD of the active cross-linker for various Péclet numbers in Fig. S2. The simulation results show that the MSD scales as $\sim t^{1/2}$ for any Pe conditions. In this supplementary analysis, we confirm this scaling behavior with the analytic expression of MSD for the active cross-linker.

In the case when all the beads in the polymer are of the same ABPs, the transformed active noise has the autocorrelation

$$\langle\tilde{\boldsymbol{\eta}}_p(t)\cdot\tilde{\boldsymbol{\eta}}_q(t')\rangle = \frac{\gamma^2 v_{\mathrm{p}}^2}{4N}\mathrm{e}^{-\frac{|t-t'|}{\tau_A}}\delta_{p,q}\left(1+\delta_{p,0}\right). \tag{S6}$$

N is the number of beads in each arm, γ the frictional coefficient of the bead, v_{p} the self-propelled velocity, and τ_A is the correlation time of the active OU noise. Compared with Eq. (13) in the main text, this transformed active noise Eq. (S6) have the same temporal correlation; however, the prefactor $1/N^2$ is changed to $1/N$, and there is no mode-couping in the active noise, i.e., $\delta_{p,q}\left(1+\delta_{p,0}\right)/2$.

Using the same mathematical techniques described in the main text, we derive the analytical expression for the ensemble-averaged MSD such that

$$\begin{aligned}\langle \Delta \mathbf{R}^2(t)\rangle = \frac{3D}{N}\left(t+\sqrt{\pi\tau_R t}\left(1-\mathrm{erf}\left(\sqrt{\frac{t}{\tau_R}}\right)\right)-\frac{3\tau_R}{2}\left(\mathrm{e}^{-\frac{t}{\tau_R}}-1\right)\right)+\frac{v_\mathrm{p}^2\tau_A^2}{N}\left(\mathrm{e}^{-\frac{t}{\tau_A}}-1+\frac{t}{\tau_A}\right)\\ +\frac{v_\mathrm{p}^2\tau_A\tau_R}{N}\left[\sqrt{\frac{\pi t}{\tau_R}}\left(1-\mathrm{erf}\left(\sqrt{\frac{t}{\tau_R}}\right)\right)+\frac{3}{2}\left(1-\mathrm{e}^{-\frac{t}{\tau_R}}\right)+\frac{\pi\left(\mathrm{e}^{-\frac{t}{\tau_A}}+\mathrm{e}^{\frac{t}{\tau_A}}-2\right)}{4\sqrt{\tau_R/\tau_A}}\right.\\ \left.-\frac{\pi}{4}\sqrt{\frac{\tau_A}{\tau_R}}\mathrm{e}^{-\frac{t}{\tau_A}}\mathrm{erfi}\left(\sqrt{\frac{t}{\tau_A}}\right)-\frac{\pi}{4}\sqrt{\frac{\tau_A}{\tau_R}}\mathrm{e}^{\frac{t}{\tau_A}}\mathrm{erf}\left(\sqrt{\frac{t}{\tau_A}}\right)+\frac{\mathrm{e}^{-\frac{t}{\tau_A}}-1}{2\left(\tau_R/\tau_A+1\right)}\right].\end{aligned} \tag{S7}$$

In Sec. IV in the main text, the dynamics of the active particle consist of three separate terms; the drift $M^{(1)}$, the Rouse dynamics $M^{(2)}$, and the active collective dynamics $M^{(3)}$. The first line of Eq. (S7) is identified to the sum of the drift motion and the Rouse dynamics, which displays $\sim t^{1/2}$ at $t \ll \tau_R$ and recovers the diffusive behavior at a later time. The Rouse dynamics term in Eq. (S7) is marginally different from the one in the main text Eq. (26) in the sense that, here, it is the ensemble-averaged Rouse dynamics while in the main text it is the dynamics only for the active cross-linker at bead index $s = 0$. The second and third lines of Eq. (S7), $M^{(3)}$, describe the collective dynamics by viscoelastic feedback of ABPs. In the limit of intermediate time scale $\tau_A \ll t \ll \tau_R$, the remaining collective dynamics $M^{(3)}$ can be written as

$$M^{(3)} \approx \left(\frac{3D}{N}+\frac{v_\mathrm{p}^2\tau_A}{N}\right)\sqrt{\pi\tau_R t} \sim t^{1/2}. \tag{S8}$$

Hence, we have demonstrated that, in the Rouse relaxation time, the collective dynamics from the active contribution scales as $\sim t^{1/2}$. Therefore, the MSD (S7) grows as $\sim t^{1/2}$ at the time scale of our interest for any Pe conditions.

C. Velocity autocorrelation of the ABP cross-linker

In this section, let us derive the analytic expressions [Eqs. (35), (36), and (37)] of the velocity autocorrelation (VACF) that discussed in the main text. The VACF can be written formally using

the normal modes as in the following:

$$
\begin{aligned}
C_v(t;\delta t) = \frac{1}{\delta t^2}\Bigg[& \langle \Delta\tilde{\mathbf{X}}_0(t+t_0;\delta t)\cdot\Delta\tilde{\mathbf{X}}_0(t_0;\delta t)\rangle \\
& + 2\sum_{p=1}^{\infty}\Big(\langle \Delta\tilde{\mathbf{X}}_0(t+t_0;\delta t)\cdot\Delta\tilde{\mathbf{X}}_p(t_0;\delta t)\rangle + \langle \Delta\tilde{\mathbf{X}}_p(t+t_0;\delta t)\cdot\Delta\tilde{\mathbf{X}}_0(t_0;\delta t)\rangle\Big)\cos\left(\frac{p\pi(s+N)}{2N}\right) \\
& + 4\sum_{p=1}^{\infty}\sum_{q=1}^{\infty}\langle \Delta\tilde{\mathbf{X}}_p(t+t_0;\delta t)\cdot\Delta\tilde{\mathbf{X}}_q(t_0;\delta t)\rangle\cos\left(\frac{p\pi(s+N)}{2N}\right)\cos\left(\frac{q\pi(s+N)}{2N}\right)\Bigg].
\end{aligned}
\tag{S9}
$$

Since all the terms in the VACF are expressed in terms of the autocorrelation of the normal modes, it is doable to analytically calculate Eq. (S9). For this, let us express $C_v(t;\delta t) = (A_1 + A_2 + A_3)/\delta t^2$, with the three terms representing each line in Eq. (S9). The first term A_1 explains the VACF for the drift of C.O.M from the active noise and reads

$$
\begin{aligned}
A_1 &= \langle \Delta\tilde{\mathbf{X}}_0(t+t_0;\delta t)\cdot\Delta\tilde{\mathbf{X}}_0(t_0;\delta t)\rangle \\
&= \frac{v_{\mathrm{p}}^2\tau_A}{2N^2}\mathrm{e}^{-\frac{t}{\tau_A}}\left[1-\cosh\left(\frac{\delta t}{\tau_A}\right)\right].
\end{aligned}
\tag{S10}
$$

As shown, this term exponentially decays out with time t, and its characteristic time is that of the active noise τ_A. For the time scale of our interest, $t \gg \tau_A$, it therefore vanishes and gives almost no effect to $C_v(t;\delta t)$. For this reason, this term is ignored in the expression of $C_v(t;\delta t)$.

We note that the expressions of A_2 and A_3 can be merged into a unified form. To show this, we calculate A_3 using the Euler-Maclaurin formula $\sum_{q=1}^{\infty} f(q) \simeq \int_0^{\infty}\mathrm{d}q f(q) - f(0)/2$. It turns out that the term $-f(0)/2$ exactly cancels out A_2. Then, the sum of the two is given by

$$
A_2 + A_3 = 4\sum_{p=1}^{\infty}\int_0^{\infty}\mathrm{d}q\,\langle \Delta\tilde{\mathbf{X}}_p(t+t_0;\delta t)\cdot\Delta\tilde{\mathbf{X}}_q(t_0;\delta t)\rangle\cos\left(\frac{p\pi(s+N)}{2N}\right)\cos\left(\frac{q\pi(s+N)}{2N}\right).
\tag{S11}
$$

Using the expression of $\langle \Delta\tilde{\mathbf{X}}_p(t)\cdot\Delta\tilde{\mathbf{X}}_q(t')\rangle$, Eq. (15) in the main text, we perform the integral in the above expression and arrive at

$$
\begin{aligned}
A_2 + A_3 = & \sum_{p=1}^{\infty}\frac{6D\tau_R}{Np^2}\mathrm{e}^{-\frac{p^2 t}{\tau_R}}\left(1-\cosh\left(\frac{\delta t}{\tau_A}\right)\right)\cos^2\left(\frac{p\pi}{2}\right) \\
& + \sum_{p=1}^{\infty}\frac{v_{\mathrm{p}}^2\tau_R\pi}{2N^2 p}\cos^2\left(\frac{p\pi}{2}\right)\mathrm{e}^{-\frac{p^2 t}{\tau_R}}\left(1-\cosh\left(\frac{\delta t}{\tau_A}\right)\right)\left(\frac{1}{p^2/\tau_R + 1/\tau_A} - \frac{1}{p^2/\tau_R - 1/\tau_A}\right) \\
& + \sum_{p=1}^{\infty}\frac{v_{\mathrm{p}}^2\tau_R\pi}{2N^2 p}\cos^2\left(\frac{p\pi}{2}\right)\mathrm{e}^{-\frac{t}{\tau_A}}\left(1-\cosh\left(\frac{\delta t}{\tau_A}\right)\right)\left(\frac{1}{p^2/\tau_R + 1/\tau_A} + \frac{1}{p^2/\tau_R - 1/\tau_A}\right).
\end{aligned}
\tag{S12}
$$

Since we are typically interested in the ABP dynamics at the time scales of $t \gg \tau_A$, the last line can be neglected compared to the first two. The first line of Eq. (S12), V_1, is evaluated to

$$\begin{aligned} V_1 &= \sum_{p=1}^{\infty} \frac{6D\tau_R}{Np^2} \mathrm{e}^{-p^2 t/\tau_R} \left(1 - \cosh\left(\frac{\delta t}{\tau_A}\right)\right) \cos^2\left(\frac{p\pi}{2}\right) \\ &= \frac{3D}{2N} \Bigg\{ \sqrt{4\pi\tau_R} \left[\sqrt{t}\, \mathrm{erfc}\left(\sqrt{\frac{4t}{\tau_R}}\right) - \frac{\sqrt{t+\delta t}}{2}\, \mathrm{erfc}\left(\sqrt{\frac{4(t+\delta t)}{\tau_R}}\right) \right. \\ &\qquad \left. - \frac{\sqrt{t-\delta t}}{2}\, \mathrm{erfc}\left(\sqrt{\frac{4(t-\delta t)}{\tau_R}}\right) \right] + \frac{3\tau_R}{2} \mathrm{e}^{-\frac{4t}{\tau_R}} \left(1 - \cosh\left(\frac{4\delta t}{\tau_A}\right)\right) \Bigg\}. \end{aligned} \tag{S13}$$

In the limits of $t \ll \tau_R$ and $\delta t \ll \tau_R$, we can simplify the expression of V_1 and finally obtain

$$\begin{aligned} V_1 &\approx \frac{3D\sqrt{\pi\tau_R}}{2N} \left[2t^{1/2} - (t+\delta t)^{1/2} - (t-\delta t)^{1/2} \right] \\ &= \frac{3D\sqrt{\pi\tau_R}}{2N} C_v^{(\mathrm{th})}(t). \end{aligned} \tag{S14}$$

Note that $C_v^{(\mathrm{th})}(t)$ is the covariance of FBM with the Hurst exponent $H = 1/4$, which is responsible for the Rouse dynamics in the MSD of the ABP cross-linker. Likewise, we can also derive the expression for the second line of Eq. (S12). For $4\tau_A \ll \tau_R$, this term, V_2, is analytically evaluated such that

$$\begin{aligned} V_2 &= \sum_{p=1}^{\infty} \frac{v_{\mathrm{p}}^2 \tau_R \pi}{2N^2 p} \cos^2\left(\frac{p\pi}{2}\right) \mathrm{e}^{\frac{-p^2 t}{\tau_R}} \left(1 - \cosh\left(\frac{\delta t}{\tau_A}\right)\right) \left(\frac{1}{p^2/\tau_R + 1/\tau_A} - \frac{1}{p^2/\tau_R - 1/\tau_A}\right) \\ &\overset{4\tau_A \ll \tau_R}{\simeq} \frac{v_{\mathrm{p}}^2 \tau_R \tau_A \pi}{8N^2} \times \\ &\quad \left[2\Gamma\left(0, \frac{4t}{\tau_R}\right) - \Gamma\left(0, \frac{4(t+\delta t)}{\tau_R}\right) - \Gamma\left(0, \frac{4(t-\delta t)}{\tau_R}\right) + \mathrm{e}^{\frac{-4t}{\tau_R}} \left(2 - 2\cosh\left(\frac{4\delta t}{\tau_R}\right)\right) \right]. \end{aligned} \tag{S15}$$

In the limits of $\delta t \ll \tau_R$ and $t \ll \tau_R$, we obtain

$$\begin{aligned} V_2 &\simeq \frac{v_{\mathrm{p}}^2 \tau_A \tau_R \pi}{8N^2} \left[\ln(t+\delta t) + \ln(t-\delta t) - 2\ln t \right] \\ &= \frac{v_{\mathrm{p}}^2 \tau_A \tau_R \pi}{8N^2} C_v^{(\mathrm{ac})}(t). \end{aligned} \tag{S16}$$

This is the VACF from the active collective motion of the ABP cross-linker, which results in the logarithmic growth of the MSD. We also find that for $t \gg \delta t$, $C_v^{(\mathrm{ac})} \sim \partial_t^2 \ln(t) \propto -t^{-2}$, showing a power-law decay with the exponent 2. Collecting Eqs. (S14) and (S16), we finally obtain the expression for the VACF as

$$C_v(t;\delta t) = \frac{\tau_R \tau_A v_{\mathrm{p}}^2 \pi}{8N^2} \left[B\, C_v^{(\mathrm{th})}(t) + C_v^{(\mathrm{ac})}(t) \right], \tag{S17}$$

where $B = 12DN/[\tau_A v_{\mathrm{p}}^2 \sqrt{\pi\tau_R}]$. This ends up the derivation of Eq. (35) in the main text.

D. Anomalous diffusion of the active cross-linker with athermal white gaussian noise

In this section, we consider a new active polymer system where the center cross-linker is modeled by an athermal noise different from the OU noise defined in Eqs. (2) and (4) in the main text. Particularly, our focus is to show that the ABP cross-linker exhibits the consistent dynamic behaviors as observed in the main text for the ABP modeled with Eqs. (1) & (2), in terms of MSD. Instead of the active OU noise, we now introduce an athermal white gasussian noise (WGN), which has $\langle \boldsymbol{\eta}(t) \rangle = 0$ and the autocorrelation

$$\langle \boldsymbol{\eta}(t) \cdot \boldsymbol{\eta}(t') \rangle = 6\gamma_A k_B T_A \delta(t-t'). \tag{S18}$$

Here, T_A is the effective temperature for the athermal WGN and γ_A is the frictional coefficient of the active particle. We repeat the Langevin dynamics simulations for this new ABP-polymer system with the athermal WGN and have investigated the MSD dynamics of the active cross-linker. Fig. S7 summarizes the results. One of the highlights is that when $T_A \gg T$ (where T is the heat bath temperature), the MSD displays a logarithmic increase in time, i.e., MSD$\sim \ln t$, as observed in the ABP cross-linker in the main text. Below we explain this with analytic analysis of the MSD.

Using the normal mode expansion and repeating the same procedure shown in the main text, we find that the MSD of the active cross-linker in this model is given by $\langle \Delta \mathbf{R}_0^2(t) \rangle = M_0^{(1)}(t) + M_0^{(2)}(t) + M_0^{(3)}(t)$, similarly to the case of the OU noise. Here, the first term in the R.H.S. describes the drift of the total system

$$M_0^{(1)} = \frac{3k_BT}{N\gamma}t + \frac{3k_BT_A}{2N^2\gamma}t, \tag{S19}$$

each of which reflecting the contribution from the thermal or active noise in the system. The second term, $M_0^{(2)}$, is responsible for the Rouse dynamics from the thermal noise and the same expression as in Eqs. (26) and (32),

$$M_0^{(2)} = \frac{3D}{2N}\left(2\sqrt{\pi\tau_R t}\left(1-\mathrm{erf}\left(\sqrt{\frac{4t}{\tau_R}}\right)\right) - \frac{3\tau_R}{2}\left(\mathrm{e}^{-\frac{4t}{\tau_R}}-1\right)\right). \tag{S20}$$

Finally, the third term is from the active collective dynamics and given by

$$\begin{aligned} M_0^{(3)} = &\sum_{p=1}^{2N} \frac{6k_BT_A\tau_R}{N^2\gamma}\cos^2\left(\frac{p\pi}{2}\right)\left[\frac{1-e^{-p^2t/\tau_R}}{p^2}\right] \\ &+ \sum_{p=1}^{2N}\sum_{q=1}^{2N} \frac{12k_BT_A\tau_R}{N^2\gamma}\cos^2\left(\frac{p\pi}{2}\right)\cos^2\left(\frac{q\pi}{2}\right)\left[\frac{1-e^{-p^2t/\tau_R}}{p^2+q^2}\right]. \end{aligned} \tag{S21}$$

In this expression, the upper limit of the summation is fixed to $2N$ to prevent the divergence of the sum (i.e., the number of the mode is $2N$). After some tedious calculations we obtain the closed-form of $M_0^{(3)}$, as in the following:

$$\begin{aligned} M_0^{(3)} &= \frac{3k_BT_A\pi\tau_R}{4N^2\gamma}\left[1-\mathrm{e}^{-\frac{4t}{\tau_R}}+2\ln N-\Gamma\left(0,\frac{4t}{\tau_R}\right)+\Gamma\left(0,\frac{4N^2t}{\tau_R}\right)\right] \\ &\approx \frac{3k_BT_A\pi\tau_R}{4N^2\gamma}\left[\gamma_E+\ln\left(\frac{4N^2t}{\tau_R}\right)\right]. \end{aligned} \tag{S22}$$

In the above, the last expression is obtained from the first line in the limit of $\tau_R/4N^2 \ll t \ll \tau_R$. Note that in Eq. (S22) $\Gamma(0,4t/\tau_R)$ behaves as $\approx -\ln(4t/\tau_R)-\gamma_E+4t/\tau_R$, where $\gamma_E = 0.5772$ is the Euler-Mascheroni constant. In this model, T_A has a similar role for v_{p}^2 in the ABP cross-linker considered in the main text. While the prefactor in Eq. (S22) linearly depends on T_A, the Rouse term $M_0^{(2)}$ does not depend on it. Therefore, in the limit of $T_A \gg T$ the active collective term $M_0^{(3)}$ dominates over $M_0^{(2)}$ in the MSD dynamics of the cross-linker, which increases logarithmically with time t. We confirm this with the simulation data shown in Fig. S7. Without a fit, the theoretical line $M_0^{(3)}(t)$ [2nd line of Eq. (S22)] successfully explains the MSD curves at high T_As.

---

[1] J. Sprakel, J. van der Gucht, M. A. Cohen Stuart and N. A. M. Besseling, *Phys. Rev. Lett.*, 2007, **99**, 208301.

[2] S. C. Chapra and R. Canale, *Numerical Methods for Engineers*, McGraw-Hill, Inc., USA, 5th edn, 2005.